Linear stability of two-dimensional combined buoyant-thermocapillary flow in cylindrical liquid bridges

M. Wanschura, H. C. Kuhlmann, and H. J. Rath
ZARM, Universität Bremen, 28359 Bremen, Germany
(Received 6 February 1997)

The combined buoyant-thermocapillary flow in cylindrical liquid bridges of unit aspect ratio is calculated by a mixed finite-difference–Chebyshev-collocation method. Gravity is assumed to be parallel or antiparallel to the cylinder's axis. For dominating thermocapillarity the two-dimensional basic flow is unique at the onset of instability. It is shown that additional buoyant body forces act stabilizing on the axisymmetric flow in high Prandtl number fluids for both heating and cooling from below. For heating from below, the onset of time-dependent convection is delayed to higher Marangoni numbers than for cooling from below, in agreement with previously unexplained experimental findings. In the absence of thermocapillary effects two axisymmetric convective solutions bifurcate from the conducting basic state. This perfect pitchfork bifurcation is perturbed by weak thermocapillary forces. The linear stability of all three axisymmetric base states is investigated numerically for Pr=4, a Prandtl number typical for model experiments. [S1063-651X(97)13906-X]

PACS number(s): 47.20.Bp, 47.20.Dr, 81.10.Fq

I. INTRODUCTION

A cylindrical volume of liquid captured between two rigid coaxial disks of equal radii and different temperatures has been frequently employed [1–4] to model certain properties of the flow occurring in the float-zone crystal-growth process [5]. This model is called half-zone model or nonisothermal liquid bridge, a sketch of which is shown in Fig. 1. It has emerged as an important paradigm for thermocapillary flows and their instabilities.

For small temperature differences ΔT imposed between the upper and lower solid boundaries the basic flow driven by thermocapillary surface forces is steady and takes the form of a single toroidal vortex, if the aspect ratio $\Gamma = d/R$ (d: height, R: radius) is of order one. A measure of the flow strength is provided by the thermocapillary Reynolds number

$$\mathrm{Re} = \frac{\gamma \Delta T d}{\rho \nu^2}, \tag{1}$$

where $\gamma = -\partial\sigma/\partial T$ denotes the negative coefficient of the surface tension σ with respect to temperature variations, ρ the mean density, and ν the kinematic viscosity. On an increase of the Reynolds or Marangoni number $\mathrm{Ma} = \mathrm{Re\,Pr}$ the flow becomes three dimensional. For small Prandtl numbers $\mathrm{Pr} = \nu/\kappa$ (κ: thermal diffusivity) in the range of $0 < \mathrm{Pr} \lesssim 0.07$ the supercritical three-dimensional flow is steady. For high Prandtl numbers $\mathrm{Pr} \gtrsim 0.5$ three-dimensional hydrothermal waves appear above the threshold Reynolds number Re_c, which propagate approximately azimuthally. While the basic thermocapillary instabilities are well known [4], the role of buoyancy measured by the Grashof number

$$\mathrm{Gr} = \frac{g \beta \Delta T d^3}{\nu^2}, \tag{2}$$

or Rayleigh number $\mathrm{Ra} = -\mathrm{PrGr}$ remains obsured. (g: acceleration of gravity, β: thermal expansion coefficient. As in most previous investigations we define $\Delta T = T(d/2) - T(-d/2) > 0$. By introducing the minus sign in the definition of the Rayleigh number, it is positive when the liquid is heated from below in agreement with the usual convention for pure buoyant flows.)Velten, Schwabe, and Scharmann [6] carried out extensive measurements of the onset of thermocapillary convection in half zones. For heating from below the critical Reynolds number for the onset of hydrothermal waves was nearly always found to be larger than that obtained during heating from above. This result is counterintuitive, since heating from above should essentially result in a stable density stratification which, from a naive point of view, should stabilize the basic two-dimensional flow.

The purpose of the present paper is to clarify the role of gravity on the onset conditions for three-dimensional flow. To that end we consider the combined buoyant-thermocapillary flow in a liquid bridge which axis is aligned parallel to the gravity vector.

The applied temperature difference ΔT is commonly used as the control parameter in experiments. Then Gr and Re

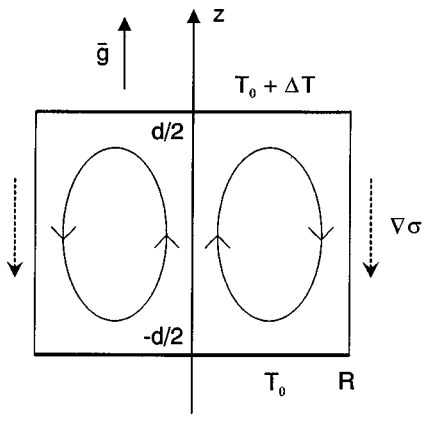

FIG. 1. Sketch of a cylindrical liquid bridge. The flow direction and thermocapillary shear stress are indicated by arrows for $\mathrm{Ra} > 0$, ($\vec{g} \uparrow\uparrow \vec{e}_z$).

TABLE I. Scales used for the nondimensionalization of the Oberbeck-Boussinesq equations.

variable	r,z	t	$\vec{u}=(u,v,w)$	p	T
scale	d	d^2/ν	$\gamma\Delta T/\rho\nu$	$\gamma\Delta T/d$	ΔT

cannot be varied independently. Their relative magnitude, the dynamic Bond number

$$\mathrm{Bd}=\frac{\mathrm{Gr}}{\mathrm{Re}}=\frac{\rho g\beta d^2}{\gamma}, \tag{3}$$

may take different values. In the experiments of Velten, Schwabe, and Scharmann [6] using liquid bridges of length $O(3\,\mathrm{mm})$, the absolute value of the Rayleigh number corresponding to the critical temperature difference for the onset of oscillatory three-dimensional flow was of the order of $|\mathrm{Ra}|\approx 1300$ for $\mathrm{Pr}=1$, $|\mathrm{Ra}|\approx 9000$ for $\mathrm{Pr}=7$, and $|\mathrm{Ra}|\approx 11\,000$ for $\mathrm{Pr}=49$. The Rayleigh numbers $|\mathrm{Ra}|$ for $\mathrm{Pr}=7$ and $\mathrm{Pr}=49$ are significantly higher than the critical Rayleigh number for the onset of pure buoyant convection [7–9]. This is taken as an indication that buoyancy forces cannot be neglected in a theoretical explanation of experimental results even for liquid bridges as short as 3 mm.

II. MATHEMATICAL FORMULATION AND NUMERICAL SOLUTION TECHNIQUE

We consider a liquid bridge of length d between two concentric rigid disks of equal radii R. In the asymptotic limit of large mean surface tension between the liquid and an ambient passive gas the location of the free surface is fixed. For a volume $V=\pi R^2 d$ it takes a straight cylindrical shape. If the disks are heated differentially with a small temperature difference ΔT the fluid motion in the liquid is governed by the Oberbeck-Boussinesq approximation

$$\partial_t\vec{u}+\mathrm{Re}\;\vec{u}\cdot\vec{\nabla}\vec{u}=-\vec{\nabla}p+\Delta\vec{u}+Bd\,\theta\vec{e}_z, \tag{4}$$

$$\vec{\nabla}\cdot\vec{u}=0, \tag{5}$$

$$\partial_t\theta+\mathrm{Re}\;\vec{u}\cdot\vec{\nabla}\theta=\frac{1}{\mathrm{Pr}}\,\Delta\theta, \tag{6}$$

where the nondimensional temperature $\theta=(T-T_0)/\Delta T$ (T_0: mean temperature) has been introduced and the variables have been made dimensionless using the characteristic scales given in Table I. The boundary conditions for an insulating free surface [4] are

$$\left.\begin{aligned}\partial_r w+\partial_z\theta&=0\\ r\partial_r\left(\frac{v}{r}\right)+\frac{1}{r}\,\partial_\varphi\theta&=0\\ u&=0\\ \partial_r\theta&=0\end{aligned}\right\}\quad\text{on}\quad r=\frac{1}{\Gamma}, \tag{7}$$

while on the rigid disks the conditions

$$\vec{u}=\vec{0},\quad \theta=\pm 1/2\quad\text{on}\quad z=\pm 1/2, \tag{8}$$

are imposed. The bridge is thus heated from above, if the acceleration of gravity is directed in negative z direction.

Decomposing the hydrodynamic fields into a steady two-dimensional solution and three-dimensional normal modes

$$\begin{pmatrix}u\\v\\w\\p\\\theta\end{pmatrix}(r,z,\varphi,t)=\begin{pmatrix}u_0\\v_0\\w_0\\p_0\\\theta_0\end{pmatrix}(r,z)+\left\{\begin{pmatrix}\hat{u}\\\hat{v}\\\hat{w}\\\hat{p}\\\hat{\Theta}\end{pmatrix}(r,z)e^{st+im\varphi}+\mathrm{c.c.}\right\}, \tag{9}$$

where c.c. denotes the complex conjugate, s is a complex growth rate, and m an integer azimuthal wave number, the linearized evolution equations for the disturbances read

$$s\vec{u}+\mathrm{Re}\{\vec{u}\cdot\vec{\nabla}\vec{u}_0+\vec{u}_0\cdot\vec{\nabla}\vec{u}\}=-\vec{\nabla}p+\Delta\vec{u}+Bd\Theta\vec{e}_z, \tag{10}$$

$$s\Theta+\mathrm{Re}\{\vec{u}\cdot\vec{\nabla}\theta_0+\vec{u}_0\cdot\vec{\nabla}\Theta\}=\frac{1}{\mathrm{Pr}}\,\Delta\Theta, \tag{11}$$

where the hats have been dropped. The steady axisymmetrical problem and the eigenvalue problem (10) and (11) have been solved with a mixed finite-difference and Chebyshev-collocation technique. Details of the numerical procedure and the validation of the code can be found in [4]. The resolutions used for the present calculations were 80 (100) finite difference points in axial direction and 20 (25) Gauss-Lobatto collocation points radially for Prandtl number 4 (0.02). With these resolutions the numerical error, defined as in [4], was kept below 5% in all cases presented.

Energy transport considerations proved valuable for the analysis of the instability mechanisms [4]. For later reference we give the Reynolds-Orr and thermal energy equation obtained by multiplying Eq. (10) by $\vec{u}$, Eq. (11) by Θ, and integrating over the volume occupied by the fluid.

$$\frac{dE_{\mathrm{kin}}}{dt}=\frac{1}{2}\,\frac{d}{dt}\int_V\vec{u}^2dV=-D+M_z+M_\varphi+I_{\mathrm{Gr}}+I_v, \tag{12}$$

$$\frac{dE_T}{dt}=\frac{1}{2}\,\frac{d}{dt}\int_V\Theta^2dV=-D_T+I_T. \tag{13}$$

The terms of viscous dissipation D, Marangoni surface work per time M_z and M_φ, and the work done by buoyant forces I_{Gr} are abbreviated as

$$D=\int_V(\vec{\nabla}\times\vec{u})^2dV-2\int_F\left(\frac{v^2}{r}\right)dF, \tag{14}$$

$$M_z=\int_F wS_{rz}dF, \tag{15}$$

$$M_\varphi = \int_F v S_{r\varphi} dF, \tag{16}$$

$$I_{\mathrm{Gr}} = \frac{\mathrm{Gr}}{\mathrm{Re}} \int_V w\Theta \, dV. \tag{17}$$

Here F denotes the free cylindrical surface and S the viscous stress tensor. The energy production terms due to interaction with the basic state are

$$I_v = \sum_{i=1}^{5} I_{vi} = -\mathrm{Re} \int_V \left(v^2 \frac{u_0}{r} + u^2 \frac{\partial u_0}{\partial r} + uw \frac{\partial u_0}{\partial z} + wu \frac{\partial w_0}{\partial r} + w^2 \frac{\partial w_0}{\partial z} \right) dV,$$

where the index i numbers the terms consecutively. Analogously, the thermal dissipation rate D_T and the thermal injection rate I_T are abbreviated,

$$D_T = \frac{1}{\mathrm{Pr}} \int_V \vec{\nabla}\Theta \cdot \vec{\nabla}\Theta dV, \tag{18}$$

$$I_T = \sum_{i=1}^{3} I_{Ti} = -\mathrm{Re} \int_V \Theta \left(u \frac{\partial \Theta_0}{\partial r} + w \frac{\partial \Theta_0}{\partial z} + w \right) dV, \tag{19}$$

where $\Theta_0 = \theta_0 - z$ is the deviation of the basic temperature field from the conductive profile. The integrals appearing in the energy equations have been computed using Simpson's rule and finite differences for the derivatives of the field quantities.

III. RESULTS

When investigating combined buoyant-thermocapillary flow instabilities it is useful to consider the limits of large and small Bond numbers separately. When the Bond number is small, the steady two-dimensional flows and their instabilities will be dominated by thermocapillarity. For large Bd on the other hand, the flow will be mainly due to buoyant convection, modified by small thermocapillary effects. The influence of the respective second driving force cannot be estimated *a priori*, since both the basic state and the neutral mode are affected in a nontrivial manner. The limit of large and small Bond numbers is therefore investigated separately for aspect ratio $\Gamma = 1$ and insulating free surface $\mathrm{Bi} = 0$. Moreover, we shall discern between small ($\mathrm{Pr} = 0.02$) and large ($\mathrm{Pr} = 4$) Prandtl numbers.

The Oberbeck-Boussinesq equations (4)–(6) and boundary conditions (7) and (8) are invariant under the transformation

$$(\mathrm{Re}, z, u, v, p) \rightarrow (-\mathrm{Re}, -z, -u, -v, -p). \tag{20}$$

It follows that the two-dimensional basic states for mixed convection ($\mathrm{Bd} \neq 0$) and their stability properties are symmetric with respect to $\mathrm{Re} = 0$. The symmetry operation (20) corresponds to a reflection of the streamlines at $z = 0$ and an inversion of the sense of rotation of the toroidal vortex (vortices). The following discussion is based on a liquid bridge heated from above. Due to the definition of the temperature difference as $\Delta T = T(d/2) - T(-d/2)$ we define the Rayleigh number as $\mathrm{Ra} = -\mathrm{Gr}\,\mathrm{Pr}$. Then $\mathrm{Ra} > 0$ for heating from below as usual. A change from a stable thermal stratification ($\mathrm{Gr} > 0$, $\mathrm{Ra} < 0$, $\vec{g} \downarrow \uparrow \vec{e}_z$) to a thermal unstable stratification ($\mathrm{Gr} < 0$, $\mathrm{Ra} > 0$, $\vec{g} \uparrow \uparrow \vec{e}_z$) may be imagined as an inversion of the $\vec{g}$ vector.

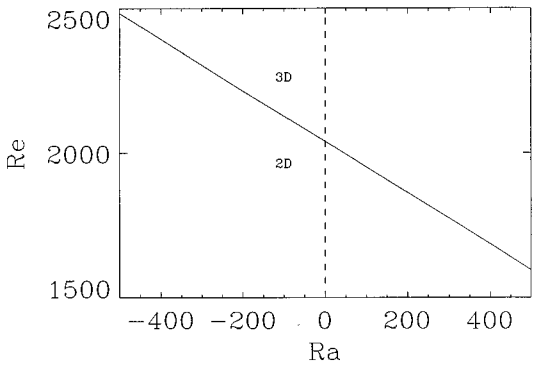

FIG. 2. Linear stability boundary Re_c as a function of the Rayleigh number for $\Gamma = 1$ and $\mathrm{Pr} = 0.02$. The critical wave number is $m = 2$.

A. Dominating thermocapillary flow

1. Pr = 0.02

For $\mathrm{Pr} = 0.02$ the range $|\mathrm{Ra}| < 500$ has been investigated. The critical mode has the wave number $m = 2$ and it is stationary as in the case of pure thermocapillary driving ($\mathrm{Ra} = 0$) (see [4]). The stability boundary as a function of Ra is shown in Fig. 2. The critical curve is nearly linear in the considered range of Rayleigh numbers. The basic state becomes destabilized for a thermally unstable density stratification ($\mathrm{Gr} < 0$, $\mathrm{Ra} > 0$), while it is stabilized for heating from above ($\mathrm{Gr} > 0$, $\mathrm{Ra} < 0$). This behavior is expected, since the basic temperature field does not deviate much from the conducting state. However, the result is not trivial.

The thermal energy balance does not vary with Ra and it is not important for this range of parameters. The kinetic energy balance for $\mathrm{Re} = 2000$ as a function of the Rayleigh number is shown in Fig. 3. Like in the pure thermocapillary case the kinetic energy transfer due to the process associated

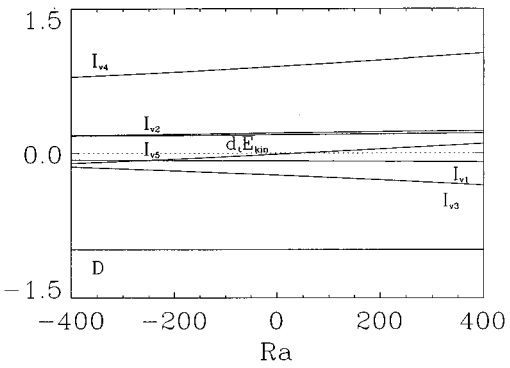

FIG. 3. Kinetic energy balance as a function of the Rayleigh number Ra for $\mathrm{Re} = 2000$, $\Gamma = 1$, and $\mathrm{Pr} = 0.02$.

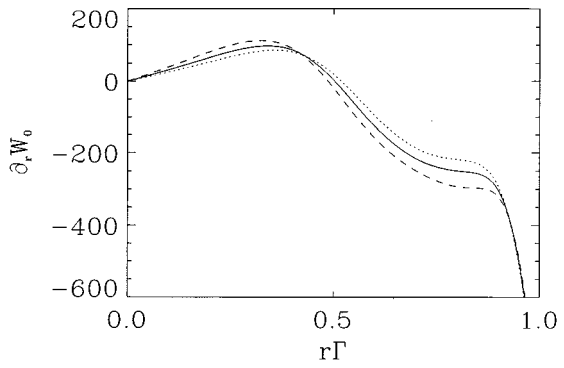

FIG. 4. Radial dependence of the shear rate $\partial_r w_0$ of the axisymmetry basic state at $z=0$ for Re=2000, $\Gamma=1$, and Pr=0.02. (—): Ra=0, (---): Ra=400, and $(\cdots)$: Ra=−400.

with I_{v4} is dominating. Therefore, the instability mechanism is inertial as for Ra=0. The work done by buoyant forces per unit of time, $I_{\mathrm{Gr}}=\mathrm{Bd}\int_V w\Theta\, dV$, is insignificant since the temperature field Θ of the neutral mode is very small. The temperature field of the basic state for Re≈2000 (not shown, cf. [4]), however, deviates notably from the conducting profile. Therefore, buoyant forces do modify the basic velocity field. As a result the absolute value of the basic shear gradient ($\partial_r w_0$) supplying the energy for the disturbance growth is reduced at the location of maximum amplification (near $r=0.75$, $z=0$, see [4]) for Ra<0 (see Fig. 4). This reduces the destabilizing energy transfer term I_{v4}. Likewise, for Ra >0, I_{v4} is enhanced compared to Ra=0. These arguments are based on the assumption that the neutral mode is unaffected by buoyancy. In fact, for the considered range of Ra the critical mode has qualitatively the same form as for Ra =0 [4].

2. Pr=4

For Pr=4 the stability boundary as a function of the Rayleigh number behaves differently. As for Ra=0 the critical mode is oscillatory with wave number $m=2$ and develops continuously from a hydrothermal wave. The stability boundary is displayed in Fig. 5 as a dashed curve. Except for a small range of Rayleigh numbers (the minimum of the

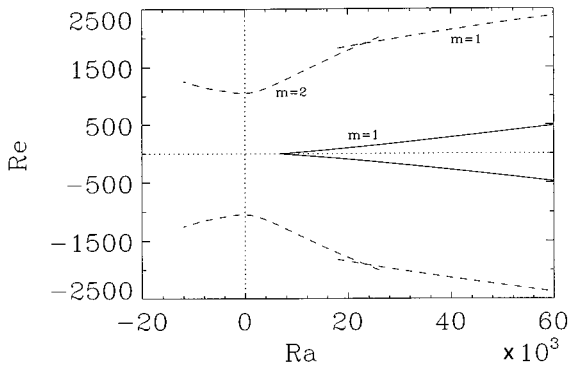

FIG. 5. Stability diagram for large Rayleigh and Reynolds numbers ($\Gamma=1$, Pr=4). For Re>0 the linearly stable range is bounded from below by a stationary ($m=1$)-instability (—). It is bounded from above by an oscillatory instability (---) with $m=2$ or $m=1$.

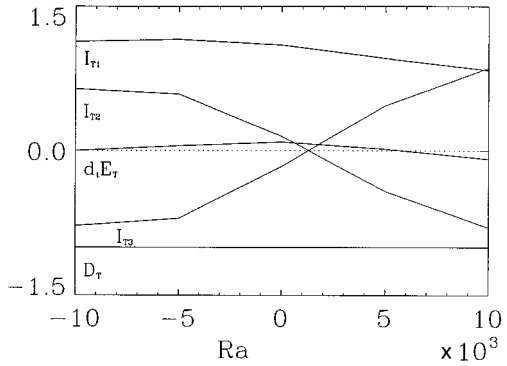

FIG. 6. Thermal energy balance as a function of the Rayleigh number Ra for Re=1200, $\Gamma=1$, and Pr=4.

critical curve is located at Ra=−360±20) buoyancy forces act stabilizing. Similar as for pure thermocapillary flow the kinetic energy balance hardly changes with the parameters (Ra). The thermal energy balance (shown in Fig. 6 for Re =1200) is important here. For Ra≈0 the contributions due to I_{T2} and I_{T3} are relatively small, but they reach the magnitude of I_{T1}, the term responsible for the appearance of hydrothermal waves, when $|\mathrm{Ra}|=10^4$. For Ra=0, the flow and temperature fields of the hydrothermal wave vary nearly exclusively in the r and φ directions and the energy is mainly transported radially. At Ra=$O(10^4)$, however, a significant amount of energy (I_{T2},I_{T3}) is transported convectively in vertical direction. This vertical transport is based on the axial component of the disturbance velocity field and couples to the basic temperature field. The coupling to the conductive part of the basic temperature field is — as expected — stabilizing for Ra<0 and destabilizing for Ra>0 (see Fig. 6). The coupling to Θ_0 (I_{T2}), however, behaves opposite. As shown by Wanschura, Kuhlmann, and Rath [9], the deviation Θ_0 of the basic temperature field from the conducting profile leads to a strong stabilization of the axisymmetric steady buoyant flow in rigid cylinders, when the liquid is heated from below (Ra>0). The same effect is present in liquid bridges. Both are strong for Ra=$O(10^4)$ but they nearly compensate each other. Since the magnitude of I_{T1} is reduced for increasing absolute values of Ra, the energy supply to the neutral mode is determined by a sensitive balance of strong opposing forces which yield a net stabilization of the basic state for Ra>0 as well as for Ra<0. Another more hand-waving explanation would be the following. Hydrothermal waves in liquid bridges are characterized by strong axial vorticity [4]. Buoyant convection on the contrary favors convection rolls with strong horizontal vorticity. Therefore, both types of convection structures are incompatible in the sense that their respective transport mechanisms exclude each other. As a consequence both modes of convection are mutually suppressed yielding a stabilization of the basic two-dimensional state.

Since the stabilization for negative Rayleigh numbers is less pronounced than that for positive Rayleigh numbers, the critical Reynolds numbers measured in terrestrial laboratories for heating from above should be less than the ones for heating from below. In fact this holds true for the measurements of Velten, Schwabe, and Scharmann [6] for fluids with Pr=1 and Pr=7. This experimental result—not explained

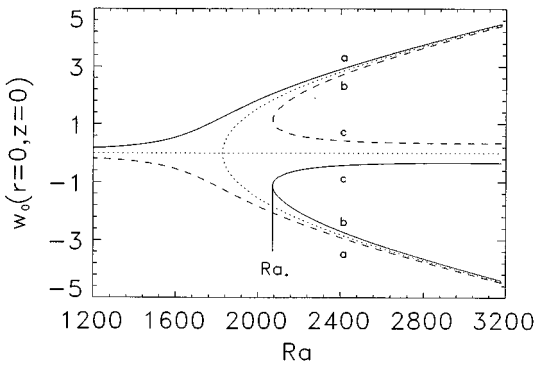

FIG. 7. Perfect bifurcation of the two-dimensional natural convection (⋯) and imperfect bifurcation due to the action of weak thermocapillary surface forces. Shown are the axial velocities in the center $w_0(r=0,z=0)$ in units of ν/d as functions of Ra for $\Gamma=1$ and Pr=4. (—): Imperfect bifurcation for Re=+5. (a), (b), and (c) denote the strong state, the weak state, and the state that develops out of the supercritical conducting solution. Ra_* is the bifurcation point of the imperfect bifurcation. (---): Imperfect bifurcation for Re=−5.

previously—can thus be understood in the framework of the stability analysis performed. Therefore, critical Reynolds numbers obtained under weightlessness conditions (Ra=0) must be smaller than those obtained in terrestrial experiments, apart from a small range of Rayleigh numbers ($-700 \lesssim \mathrm{Ra} < 0$ for Pr=4) around the minimum of $\mathrm{Re}_c(\mathrm{Ra})$. This conclusion is in qualitative agreement with recent drop tower experiments [10] in which the onset of thermocapillary induced flow oscillations have been observed after a high Prandtl number liquid bridge was subjected to a sudden transition from $1g$ to $\approx 0g$.

B. Dominating buoyant flow

The stability map for dominating buoyancy is more complicated. The main reason is that up to three different two-dimensional basic flow states may exist. The typical bifurcation structures are discussed here for $\Gamma=1$ and Pr=4.

Let us first consider only two-dimensional flows regardless of their stability with respect to three-dimensional perturbations. For Re=0 the conductive state ($\vec{u}_0=\Theta_0=0$) becomes linearly unstable to a two-dimensional mode at $\mathrm{Ra}_c(m=0)=1825$ via a perfect pitchfork bifurcation (see [9]). This bifurcation is shown as a dotted line in Fig. 7. For $\mathrm{Ra}>\mathrm{Ra}_c(m=0)$ there exist two equivalent supercritical convective solutions representing flow states with up or downflow at the center ($r=z=0$) of the liquid bridge in addition to the unstable conducting state.

If Re≠0 a structural instability [11] occurs and the bifurcation becomes imperfect. The imperfect bifurcation for Re =+5 is drawn as full lines in Fig. 7. For a thermally unstable stratification (Ra>0) the preferred two-dimensional convective state has upflow in the center if Re>0. This state will be called *strong state* (a) in the following. The corresponding flow field consists of a single toroidal vortex, which sense of rotation is supported by both buoyant and thermocapillary forces (see Fig. 1; Fig. 8 applies to Re=−5. For Re>0 the streamlines must be reflected at $z=0$.). For Rayleigh numbers larger than the value $\mathrm{Ra}_*(\mathrm{Re}) \geqslant \mathrm{Ra}_c(m=0)$, which depends on Re, there exist two more solutions, the *weak state* (b), and a state (c) (Fig. 8), which are identical at $\mathrm{Ra}=\mathrm{Ra}_*$. In both latter states buoyant and thermocapillary forces are opposing in the sense that they favor different directions of vortex motion. As a result, two additional small vortices appear in the hot and the cold corner where the buoyant convection is weak and thermocapillary forces are strong. The small corner vortices are thermocapillary in ori-

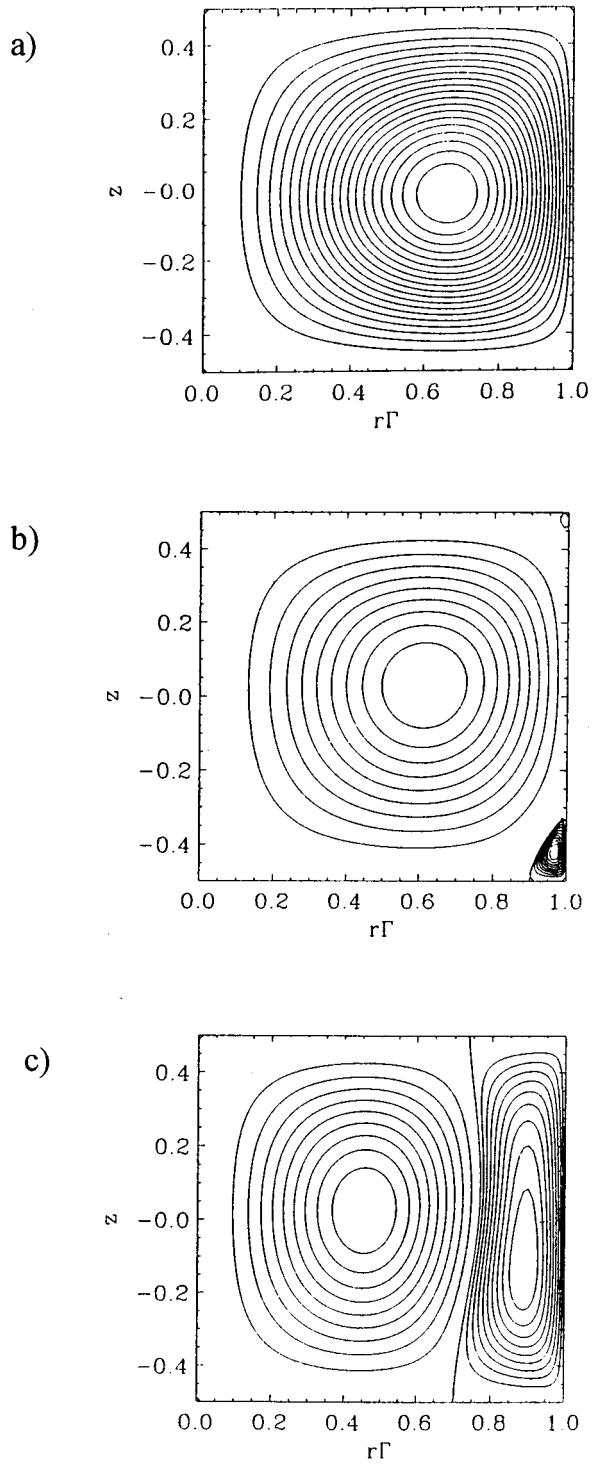

FIG. 8. Three different axisymmetric basic flow solutions for Ra=3200, Re=−5, Pr=4, and $\Gamma=1$.

gin and the flow is circulating opposite to the flow in the large vortex of buoyant origin in the bulk. The weak state (b) [corresponding to Fig. 8(b)] is characterized by a strong internal toroidal vortex which sense of rotation (downward flow at $r=z=0$ for Re$>$0) is determined by buoyancy. On an increase of Ra both thermocapillary corner vortices are suppressed and only very small corner vortices remain. The larger of these corner vortices is always located downstream the surface flow owing to the large buoyant vortex, i.e., at the hot corner for Re$>$0 and at the cold corner for Re$<$0. For very high Rayleigh numbers the corner vortices may eventually vanish. Flow state (c) [corresponding to Fig. 8(c)] has developed out of the supercritical conducting state on an increase of Re. Contrary to the states (a) and (b) its temperature field deviates least from the conducting profile. State (c) is associated with the smallest Nusselt number, whereas the Nusselt number is largest for the strong state (a). On an increase of Ra beyond Ra_* the thermocapillary corner vortices for state (c) grow and finally merge to form a single thermocapillary vortex confined to a layer below the free surface. In the interior remains a weak buoyancy driven vortex with opposite sense of rotation.

For an increasing Rayleigh number and zero Reynolds number there exists an infinite sequence of successive pitchfork bifurcations out of the conducting state. The respective two-dimensional neutral modes possess an increasing number of radial nodes. In the presence of a small imperfection due to a nonzero Reynolds number the branch (a) of order $n+1$ becomes connected with the type-c solution branch of order n. These higher two-dimensional bifurcations are, however, not investigated here, because the corresponding solutions are most likely to be unstable with respect to three-dimensional disturbances.

Due to the invariance (20) of the Oberbeck-Boussinesq equations all two-dimensional vortex states are symmetric with respect to Re$=$0. The imperfect bifurcation for Re$<$0 is shown in Fig. 7 as dashed lines. On a continuous decrease of the Reynolds number from positive to negative values the solution corresponding to the weak state (b) transforms smoothly into the solution belonging to the strong state (a) and vice versa.

The boundary $\mathrm{Ra}=\mathrm{Ra}_*(\mathrm{Re})$ of the parameter range for which all three nontrivial two-dimensional basic states (a, b, and c) exist is shown as a dotted line in Fig. 9. The linear stability analysis shows that state (c) is always unstable, even with respect to two-dimensional perturbations. All neutral modes of the basic states (a) and (b) are stationary along the neutral curves shown in Fig. 9.

For Pr$=$4 and $\Gamma=1$ the first instability for Re$=$0 is three dimensional with $m=2$ at $\mathrm{Ra}_c(m=2)=1616$ [9]. Since $\mathrm{Ra}_c(m=2)$ is smaller than $\mathrm{Ra}_c(m=0)$ by a finite amount this instability corresponds to the instability of the strong state [The weak state can only exist for $\mathrm{Ra}>\mathrm{Ra}_c(m=0)$]. On an increase of the Rayleigh number (Re$=$0) the linear growth rate of infinitesimal perturbations of the strong state becomes larger, reaches a maximum, and vanishes again at $\mathrm{Ra}_c'(m=2)=3586>\mathrm{Ra}_c(m=0)$. The strong axisymmetric basic state is linearly stable immediately above $\mathrm{Ra}=\mathrm{Ra}_c'(m=2)$. Both bifurcation points at Re$=$0 are connected in the (Re,Ra) plane by the critical curve for $m=2$ of the strong

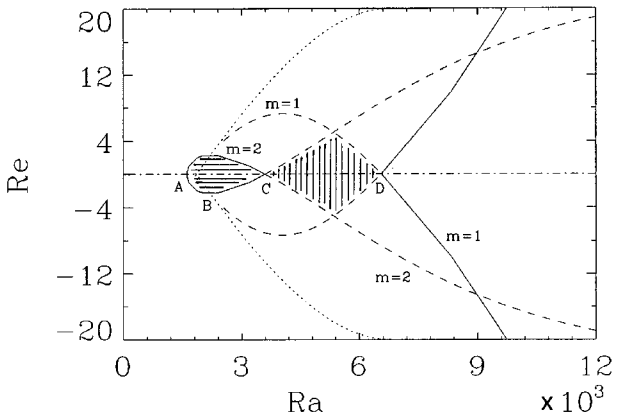

FIG. 9. Stability chart for $\Gamma=1$ and Pr$=$4. (⋯): Ra_*; (—): Linear stability boundaries of the strong state (a); (—): Linear stability boundaries of the weak state (b). In the horizontally shaded area and to the right of the full ($m=1$) curve the strong state is unstable; it is linearly stable otherwise. In the vertically shaded area the weak state is linearly stable; it is unstable otherwise. The capital letter denote: (A): $\mathrm{Ra}_c(m=2)=1616$, (B): $\mathrm{Ra}_c(m=0)=1825$, (C): $\mathrm{Ra}_c'(m=2)=3586$, and (D): $Ra_{c2}(m=1)=6557$.

state. Since the sign of the growth rate is preserved along both sides of the critical curve, the strong state is unstable with respect to $m=2$ disturbances only inside the horizontally shaded closed area (see Fig. 9).

If, for $\mathrm{Ra}_*(\mathrm{Re}=0)<\mathrm{Ra}<\mathrm{Ra}_c'(m=2)$, the line Re$=$0 is crossed from either negative or positive Reynolds numbers, the strong state solution transforms into the weak state solution. Since the disturbance growth rate is finite on the axis Re$=$0, both the strong and the weak state are linearly unstable in a vicinity of the Re$=$0 axis. While the real part of the disturbance growth rates for the strong states cross zero on the full $m=2$ curve in Fig. 9, the growth rate of the weak states remain positive. Therefore, the weak states are also linearly unstable directly outside the horizontally shaded area.

As the neutral stability boundaries of the strong states with respect to $m=2$ modes are followed for higher Rayleigh numbers crossing $\mathrm{Ra}_c'(m=2)=6557$, the neutral curves apply to the stability of the weak states. Therefore, the weak states are linearly stable within the vertically hatched area which is also bounded by a neutral curve corresponding to a mode with $m=1$. Due to the same argument as given above also the strong states are linearly stable in the vertically hatched area, but they are also linearly stable outside of it.

In a vicinity of Re$=$0 and for $\mathrm{Ra}>\mathrm{Ra}_{c2}(m=1)$ the roles of the strong and weak states are reversed once again. Therefore, the strong state is unstable to an $m=1$ mode for Rayleigh numbers that are larger than the values indicated by the solid $m=1$ curve in Fig. 9. The weak states are all linearly unstable for $\mathrm{Ra}>\mathrm{Ra}_{c2}(m=1)$ regardless of the Reynolds number. The $m=1$ curve terminates on the existence boundary of the weak state (dotted).

From Fig. 9 two interesting general properties can be extracted. The three-dimensional buoyant convection for $\mathrm{Ra}>\mathrm{Ra}_c(m=2)$ with basic mode $m=2$ is suppressed by even weak ($|\mathrm{Re}|<4$) thermocapillary effects. Moreover,

there exists a range of Rayleigh numbers $\mathrm{Ra}>\mathrm{Ra}_c'(m=2)$, for which the axisymmetric convection is linearly restabilized and where for $\mathrm{Re}\neq 0$ two different axisymmetric states (a) and (b) exist. Both states should be realizable in the absence of finite amplitude instabilities.

IV. CONCLUDING REMARKS

The continuation of the $(m=1)$-stability boundaries of the strong state with respect to both stationary and oscillatory modes is depicted in Fig. 5. For large Rayleigh numbers, there always exists an interval of Reynolds numbers for which the two-dimensional (strong) basic state is linearly stable. On the scale of Fig. 5 the Reynolds numbers that limit the linearly stable range from below and from above depend nearly linearly on the Rayleigh number. If the linear instabilities of the axisymmetric base state are supercritical, three-dimensional flow could be suppressed even for large Rayleigh numbers by moderate thermocapillary effects. Note that within the Oberbeck-Boussinesq approximation the Re, Ra plane is traversed along a ray originating from the origin $(\mathrm{Re}=\mathrm{Ra}=0)$ with a slope given by $\mathrm{Bd}^{-1}\mathrm{Pr}^{-1}$, when the temperature is varied as in experiments. An experimental verification of the stability boundaries found is still lacking. The range of complex bifurcation behavior around $\mathrm{Ra}\approx 4000$ for $\mathrm{Pr}=4$, however, seems to be accessible through experiments with small volume liquid bridges (cf. experiments by Velten, Schwabe, and Scharmann [6]), if test liquids with small thermocapillary effect are employed. Such experiments could also settle the question for a possible hysteretic behavior, which cannot be answered within the present linear analysis.

ACKNOWLEDGMENT

This work has been supported by Deutsche Forschungsgemeinschaft under Grant No. Ku896/2-2.

[1] F. Preisser, D. Schwabe, and A. Scharmann, J. Fluid Mech. **126**, 545 (1983).
[2] H. C. Kuhlmann and H. J. Rath, J. Fluid Mech. **247**, 247 (1993).
[3] G. P. Neitzel, K.-T. Chang, D. F. Jankowski, and H. D. Mittelmann, Phys. Fluids A **5**, 108 (1993).
[4] M. Wanschura, V. M. Shevtsova, H. C. Kuhlmann, and H. J. Rath, Phys. Fluids **7**, 912 (1995).
[5] *Handbook of Crystal Growth*, edited by D. T. J. Hurle (North-Holland, Amsterdam, 1994).
[6] R. Velten, D. Schwabe, and A. Scharmann, Phys. Fluids A **3**, 267 (1991).
[7] G. S. Charlson and R. L. Sani, Int. J. Heat Mass Transfer **13**, 1479 (1970).
[8] G. S. Charlson and R. L. Sani, Int. J. Heat Mass Transfer **14**, 2157 (1971).
[9] M. Wanschura, H. C. Kuhlmann, and H. J. Rath, J. Fluid Mech. **326**, 399 (1996).
[10] M. Sakurai (private communication).
[11] P. G. Drazin, *Nonlinear Systems* (Cambridge University Press, Cambridge, England, 1992).